H+O3 Fouriertransform infrared emission and laser absorption studies of OH (X 2Π) radical: An experimental dipole moment function and statetostate Einstein A coefficients

David D. Nelson Jr., Aram Schiffman, David J. Nesbitt, John J. Orlando, and James B. Burkholder

Citation: The Journal of Chemical Physics **93**, 7003 (1990); doi: 10.1063/1.459476
View online: http://dx.doi.org/10.1063/1.459476
View Table of Contents: http://scitation.aip.org/content/aip/journal/jcp/93/10?ver=pdfcov
Published by the AIP Publishing

$H+O_3$ Fourier-transform infrared emission and laser absorption studies of OH ($X\,^2\Pi$) radical: An experimental dipole moment function and state-to-state Einstein A coefficients

David D. Nelson, Jr.,[a] Aram Schiffman, and David J. Nesbitt[b]
Joint Institute for Laboratory Astrophysics, University of Colorado and National Institute of Standards and Technology, and Department of Chemistry and Biochemistry, University of Colorado, Boulder, Colorado 80309-0440

John J. Orlando and James B. Burkholder
NOAA Aeronomy Laboratory, R/E/AL2, 325 Broadway, Boulder, Colorado 80303 and Cooperative Institute for Research in Environmental Sciences, University of Colorado, Boulder, Colorado

(Received 22 June 1990; accepted 7 August 1990)

The relative intensities of 88 pairs of rovibrational transitions of OH ($X\,^2\Pi$) distributed over 16 vibrational bands ($v' \leqslant 9$, $\Delta v = -1, -2$) have been measured using Fourier transform infrared (FTIR) emission/absorption spectroscopy. Each pair of transitions originates from a common vibrational, rotational, and spin–orbit state, so that the measured relative intensities are *independent* of the OH number density and quantum state distribution. These data are combined with previous $v = 1 \leftarrow 0$ relative intensity absorption measurements and $v = 0$, 1, and 2 permanent dipole moments to determine the OH dipole moment function as a cubic polynomial expanded about r_e, the equilibrium bond length. The relative intensities provide detailed information about the shape of the OH dipole moment function $\mu(r)$ and hence the *absolute* Einstein A coefficients. The intensity information is inverted through a procedure which takes full account of the strong rotation–vibration interaction and spin uncoupling effects in OH to obtain the dipole moment function (with 95% confidence limits): $\mu(r) = 1.6502(2)\ \mathrm{D} + 0.538(29)\ \mathrm{D/\AA}\ (r - r_e) - 0.796(51)\ \mathrm{D/\AA^2}\ (r - r_e)^2 - 0.739(50)\ \mathrm{D/\AA^3}\ (r - r_e)$,[3] with a range of quantitative validity up to the classical turning points of the $v = 9$ vibrational level (i.e., from 0.70 to 1.76 Å). The $\mu(r)$ determined in this study differs significantly from previous empirical analyses which neglect the strong effects of rotation–vibration interaction and spin uncoupling. The present work also permits distinguishing between the various *ab initio* efforts. Best agreement is with the dipole moment function of Langhoff, Werner, and Rosmus [J. Mol. Spectrosc. **118**, 507 (1986)], but their theoretical predictions for higher overtone transitions are still outside of the 2σ experimental error bars. Absolute Einstein A coefficients from the present $\mu(r)$ are therefore presented for P, Q, R branch transitions for $\Delta v = 1$, 2, 3, $v' \leqslant 9$, $J' \leqslant 14.5$, in order to provide the most reliable experimental numbers for modeling of near IR atmosphere OH emission phenomena.

I. INTRODUCTION

The OH Meinel emission bands were first observed in the night sky nearly 40 years ago.[1] This emission arises from ($v \leqslant 9$) vibrationally excited OH radicals which radiate on a series of fundamental and overtone transitions following its production from the reaction of $H + O_3$. The radiated light intensity provides a direct measure of the OH quantum state distribution in the mesosphere *if* one knows the Einstein A coefficients governing the emission. The OH populations deduced in this manner are used to model the temperature of the mesosphere and can potentially yield insight into the H atom chemistry in this region of the atmosphere.[2,3] There are many other important applications of the OH vibrational emission spectrum. For example, recent laboratory measurements of the branching ratios in de-NO_x processes depend directly on the $v = 1 \rightarrow 0$ Einstein A coefficients.[4] Flash kinetic infrared measurements of the absolute OH quantum yield in the ultraviolet photolysis of HNO_3 also rely on the Einstein A coefficients.[5] In addition, the OH vibrational spectrum is used to determine the solar oxygen abundance,[6] to probe the temperature structure of the solar photosphere,[6] and to investigate the chemical composition of red giant stars.[7] The general importance of the OH Einstein A coefficients has motivated a longstanding effort to measure them experimentally as well as to calculate them from first principles.

Two special properties of the OH radical make the determination of Einstein A coefficients particularly challenging. First, the OH radical exhibits intense overtone transitions in the Meinel bands so that Einstein A coefficients for $\Delta v = 1$–4 transitions with $v' = 1$–9 are important. This unusual situation arises because the OH dipole moment function has large curvature near r_e and, in fact, passes through its

[a] National Research Council Fellow. Present address: Aerodyne Research, Inc., Billerica, Massachusetts.
[b] Staff member, Quantum Physics Division, National Institute of Standards and Technology.

maximum at a small displacement from r_e. This maximum occurs at approximately the $v=2$ outer classical turning point and the resulting curvature in $\mu(r)$ makes the high v *overtone* transitions stronger than the $\Delta v=1$ *fundamental* transitions. The second factor is that rotation–vibration interaction and spin uncoupling strongly modify the infrared transition strengths in OH as a function of rotation. OH has a large permanent dipole moment ($\sim$1.7 D) but a small vibrational transition dipole moment ($\sim$0.01–0.03 D) which tends to accentuate the rotation–vibration interaction effects on the Einstein A coefficients. This phenomenon is further emphasized because OH is a diatomic hydride with a large rotational constant ($B_e \approx 18.91\text{cm}^{-1}$), and which therefore maximizes centrifugal distortion of the OH bond even for relatively low J. Spin uncoupling effects are large and strongly J dependent in this open shell system since it is intermediate between Hund's case **a** and Hund's case **b** electronic angular momentum coupling schemes. As a result of these strong rotational modifications of the transition intensities, most vibrational bands are poorly described by a single Einstein A coefficient. Thus, thousands of individual rovibronic transition strengths are necessary to characterize the emission behavior from a distribution of OH rotational and vibrational quantum states.

General approaches to this problem have, therefore, focused on the calculation of the OH dipole moment function $\mu(r)$ from which all the transition intensities can be determined. Early experimental approaches were pioneered by Garvin *et al.*[8] and by Murphy.[9] These workers deduced empirical dipole moment functions based primarily on the relative intensities of different overtone transitions originating from the same vibrational state, i.e., $\Delta v=(n-1)/\Delta v=n$ intensity ratios. In these early efforts the rotational dependence of the transition intensities was either ignored or minimized by approximate techniques. As a result of sensitivity and/or resolution limitations, this approximation is often still used. For example, the recent empirical dipole moment function of Turnbull and Lowe[10] is also based on $\Delta v=(n-1)/\Delta v=n$ intensity ratios, where most of the ratios are simply averaged over J due to signal-to-noise limitations. However, this represents a loss of significant information since the rotational dependence of the $\Delta v=1$ transitions, in particular, is quite strong and provides a sensitive measure of the local (i.e., vibrationally averaged) *slope* of $\mu(r)$ which is otherwise difficult to obtain (*vide infra*).

Early *ab initio* calculations of the OH dipole moment function were performed by Meyer[11] and by Stevens *et al.*[12] Mies calculated Einstein A coefficients from the dipole moment function of Stevens *et al.*[12] which for many years have been accepted as the best available values.[13] Recent *ab initio* efforts include the dipole moment functions of Langhoff *et al.*[14,15] These functions are similar to each other, but differ strongly from the work of Stevens *et al.*[12] and Turnbull and Lowe.[10] In fact, the functions discussed above predict Einstein A coefficients which differ by up to twofold in many cases. In light of this, the determination of $\mu(r)$ is by no means a closed issue.

In an earlier work we presented a dipole moment function for OH based on concentration independent flash kinetic absorption measurements[4] within $v=1\leftarrow 0$ in conjunction with permanent dipole moment measurements[16] in $v=0$, 1, and 2. The absorption measurements determine the relative intensities of transitions originating from a common vibrational, rotational, spin–orbit, and lambda doublet state. These ratios and dipole moments are inverted through a procedure which takes full account of rotation–vibration interaction and spin uncoupling[17] to obtain a cubic polynomial representation of $\mu(r)$ optimized in a least squares sense. The $v=1\leftarrow 0$ intensity ratios are quite sensitive in zeroth order to the *slope* of $\mu(r)$ near r_e, vibrationally averaged over the region sampled by the $v=0$ and 1 wave functions. This sensitivity proves to be a key feature of the present analysis which is not provided solely from $\Delta v=(n-1)/\Delta v=n$ intensity ratios. Conversely, the permanent dipole moment measurements are most sensitive to the *magnitude* of $\mu(r)$ near r_e. Hence the slope and magnitude of $\mu(r)$ are experimentally well determined near r_e, which permits accurate calculation of the Einstein A coefficients for $\Delta v=1,2$ transitions in the lowest vibrational states. However, since our previous experimental data only sample $\mu(r)$ between the $v=2$ classical turning points (0.80–1.26 Å), predictions for states with $v>3$ remain uncertain.

In this work we extend the previous results to much higher vibrational levels by exploiting high resolution *emission* rather than *absorption* methods. We report here the measurement of relative vibration–rotation transition intensities in chemiluminescence of vibrationally excited OH, formed from the reaction of H atoms with O_3. Intensity ratios are measured by Fourier transform infrared spectroscopy and include states with $v'\leqslant 9$. The high sensitivity of these measurements achieves signal-to-noise ratios approaching 200 on the strongest transitions. The data set provided by these studies is sensitive to the dipole moment function throughout the region bounded by the $v=9$ classical turning points, the region of greatest interest for atmospheric investigations.

These measurements are used to extract an extended version of our earlier dipole moment function.[5] The new function falls within reported uncertainties of our previous $\mu(r)$, but is now accurate from 0.70–1.76 Å, (i.e., the $v=9$ classical turning points) and has uncertainties over this region which are substantially reduced from those of the earlier function. Furthermore, the function is highly overdetermined by the data (97 relative intensities and 3 permanent dipole moments to fit M_0, M_1, M_2, and M_3) which permits a series of tests for internal consistency in the analysis. The refined dipole moment function is used to calculate P, Q, and R branch Einstein A coefficients for $\Delta v=1$–3 transitions with $v'\leqslant 9$. The typical uncertainty in these experimentally determined A factors is $\leqslant 10\%$ for strong transitions, and provides the most reliable Einstein A coefficients available for characterization of OH atmospheric emission and absorption phenomena.

The organization of this paper is as follows. In Sec. II we discuss the experimental technique used to obtain the Einstein A ratios. We present the observed intensity ratios and discuss their uncertainties in Sec. III. In Sec. IV we give the dipole moment function which follows from the intensity

ratios along with Einstein A coefficients calculated from $\mu(r)$. Given the considerable importance of these OH radiative rates, the Einstein A coefficients for transitions with $v' < 10, \Delta v = 1\text{–}3, J' < 14.5, \Delta J = 0, \pm 1$ and $F' = F'' = 1,2$ are tabulated. In Sec. V we discuss the dipole moment function and transition strengths presented in this paper and compare them with the results of previous theoretical and empirical efforts. Section VI presents further experimental checks of the internal consistency of the data analysis, while Sec. VII concludes and summarizes the paper.

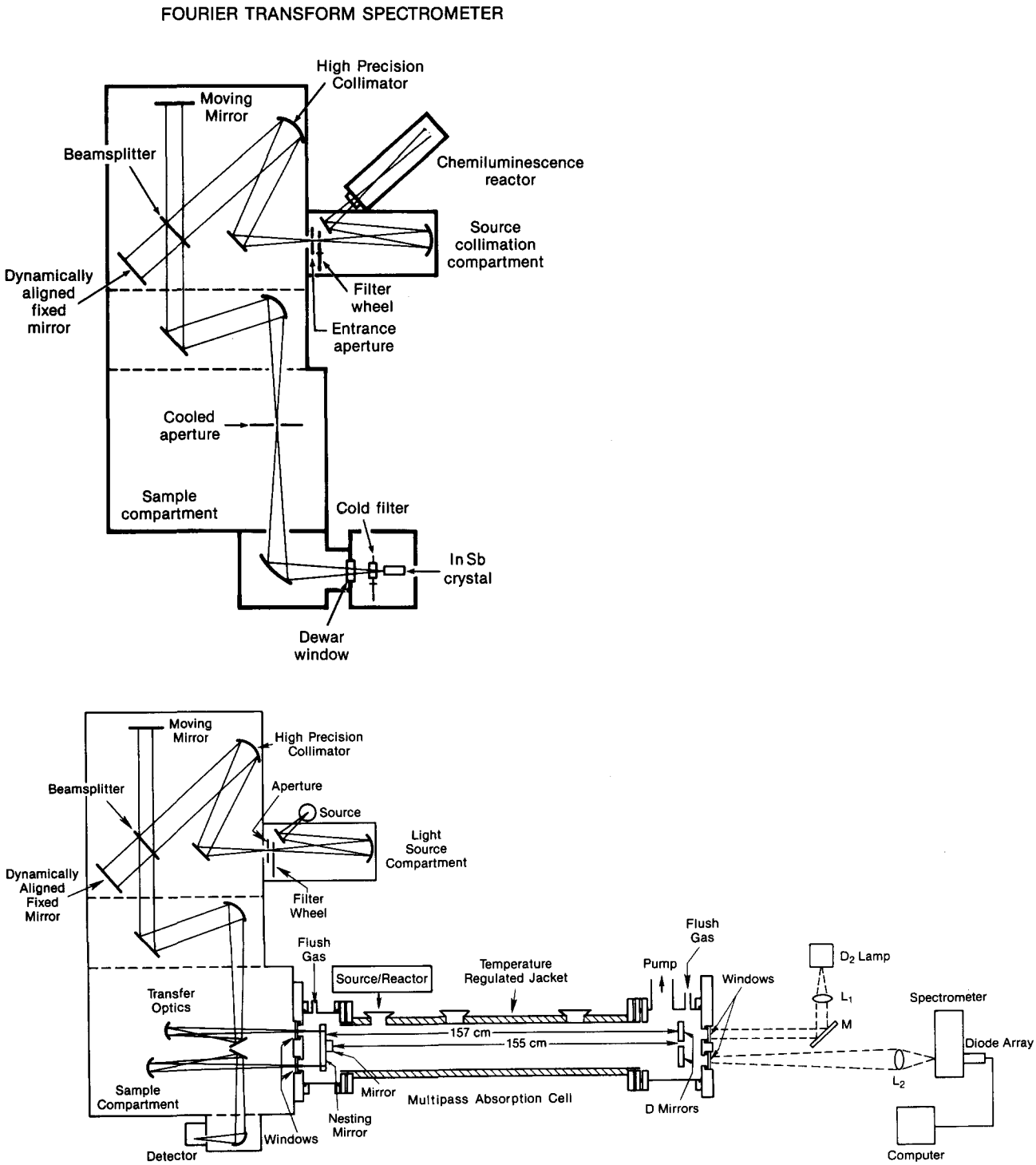

FIG. 1. Fourier transform spectrometer: (a) configuration for OH vibrational emission measurements; (b) configuration for OH $v = 1$–0 band absorption measurements.

II. EXPERIMENTAL

An overview of the Fourier transform spectrometer (FTS) is shown in Fig. 1. Detailed descriptions of its operation and performance characteristics are presented elsewhere.[18] We first discuss the details of the emission measurements which comprise the bulk of this work. The infrared chemiluminescence is detected by a liquid nitrogen cooled InSb photodiode followed by a low noise transimpedance amplifier. The spectra obtained span the region from 1975 to 7200 cm^{-1} with a CaF_2 beamsplitter used throughout. The window of the emission cell is KBr. Fifteen individual spectra are collected with acquisition times which vary from ~40–75 min. For most scans the spectral resolution is 0.05 cm^{-1}. The highest signal-to-noise ratios (~200:1 on strong lines) are obtained in the $\Delta v = 1$ scans with $v' < 8$ where a liquid nitrogen cooled 4.5 μm short pass filter is employed. This filter reduces broad band noise on the detector by limiting background blackbody radiation from the FTS. Alternatively, scans acquired without this filter took advantage of a dry ice cooled aperture placed at the first image of the entrance aperture to reduce background radiation. Table I summarizes the details of each scan including the frequency range, the vibrational bands obtained, the spectrometer resolution, and the status of the 4.5 μm cold filter. For all scans, aperture sizes are chosen according to spectral range and resolution requirements. For all emission spectra the aperture diameter is 3.5 mm. The phase characterization of the interferograms is carried out using a quartz halogen lamp placed inside the emission cell. The interior of the spectrometer is purged with He or dry N_2 to eliminate infrared absorbing species in the beam path.

The OH is formed in the emission cell by the reaction of H atoms with ozone. The essential chemistry is described below

$$H_2 \xrightarrow{\text{discharge}} H + H, \tag{1}$$

$$H + O_3 \rightarrow OH^{\ddagger}(v \leqslant 9) + O_2, \tag{2}$$

$$OH^{\ddagger} + M \rightarrow OH + M, \tag{3}$$

$$OH^{\ddagger} \rightarrow OH + h\nu, \tag{4}$$

where ‡ denotes vibrational excitation. The enthalpy of the $H + O_3$ reaction ($\Delta H = -322$ kJ/mol[19]) is sufficient to populate the OH ($v = 9$) level from room temperature reactants. It is clearly important in these experiments to minimize the vibrational relaxation of the OH radicals during their ~10 ms residence in the emission cell. H atoms are the most efficient relaxer present with $k_3(v = 1,2) = 3 \times 10^{-10}$ cm^3 molecule s^{-1}.[22] It is therefore reasonable that the best results should be obtained with an excess of ozone (with respect to H) flowing into the emission cell. Indeed, excess ozone does produce optimal signal strength and our signals continue to increase with increased ozone flow up to the highest flow rates utilized. We estimate the OH formation time in our emission cell as ~200 μs ($k_2 = 2.8 \times 10^{-11}$ cm^3 molecule^{-1} s^{-1}).[19] If the vibrational relaxation of OH by H atoms proceeds at a near gas kinetic rate for all v, the relaxation process would also occur on a 200 μs time scale, thus explaining our sensitivity to ozone concentration.

Optimal experimental conditions for recording the OH emission data are as follows. The total pressure in the emission cell is 0.6 Torr (1 Torr = 133 Pa), 99% of which is He carrier gas. The total input flow rate is 20 STP cm^3 s^{-1} (STP: 760 Torr, 273 K). The initial ozone concentration is $\sim 2 \times 10^{14}$ molecule cm^{-3} whereas the initial H atom concentration is estimated at $\sim 2 \times 10^{13}$ molecule cm^{-3}, based on 50% dissociation of the H_2 in the microwave discharge. The residence time of the gases in the spectrometer field of

TABLE I. Conditions for acquisition of FTIR spectra.

Scan	Type[a]	Acquisition time (min.)	Filter status[b]	Resolution (cm^{-1})	Frequency range (cm^{-1})	Vibrational bands
1	E	40	N	0.05	2850–3450	4→3,3→2
2	E	40	N	0.05	2500–3100	6→5,5→4
3	E	40	N	0.05	2035–2635	9→8,8→7
4	E	40	N	0.05	1975–2565	9→8,8→7
5	E	40	H	0.05	2350–3200	7→6,6→5,5→4
6	E	40	H	0.05	2720–3425	5→4,4→3
7	E	40	H	0.05	2800–3445	4→3,3→2
8	E	40	H	0.05	3050–3850	2→1,1→0
9	E	40	H	0.05	2350–3200	7→6,6→5,5→4
10	E	40	H	0.05	2720–3425	5→4,4→3
11	E	40	H	0.05	2800–3445	4→3,3→2
12	E	40	H	0.05	3050–3850	2→1,1→0
13	E	40	H	0.05	3050–3850	2→1,1→0
14	E	75	N	0.10	2000–7200	$\Delta v = 1, \Delta v = 2$[c]
15	E	75	N	0.10	2000–7200	$\Delta v = 1, \Delta v = 2$[c]
16	A	170	L	0.01	3520–3900	1←0

[a] E(A) indicates Fourier transform emission (absorption) scan.
[b] H indicates that the liquid nitrogen cooled 4.5 μm high pass filter was employed; L indicates the use of the room temperature 2.5 μm low pass filter. N implies that no filtering was used.
[c] All $\Delta v = 1$ and $\Delta v = 2$ band origins with $v' < 10$ are covered in this scan.

view is roughly ~ 10 ms. Figure 2 shows a typical emission spectrum recorded.

In addition to measuring OH vibrational emission, the FTS was also used for remeasuring $v = 1 \leftarrow 0$ absorption intensity ratios from a more nearly room temperature OH ($v = 0$) source. This provides an additional redundancy check on the intensity ratios determined previously by flash kinetic spectroscopy methods.[5] The OH radicals for the absorption experiment are formed by the reaction of F atoms with H_2O:

$$F_2 \xrightarrow{\text{discharge}} 2F \tag{5}$$

$$F + H_2O \rightarrow HF + OH. \tag{6}$$

Although this reaction is sufficiently exothermic to populate OH $v = 1$,[23] the observed spectra are consistent with a near room temperature OH rovibrational distribution. The total pressure in the absorption cell is 0.75 Torr and the total flow rate is 130 STP $cm^3\ s^{-1}$, resulting in a much larger OH residence time in the cell of ~ 100 ms. The H_2O is carried into the cell by flowing He gas through a H_2O bubbler. The initial H_2O concentration is estimated at $\sim 2\times 10^{14}$ molecule cm^{-3} based on the partial pressure of H_2O in the He/H_2O mixture and the flow rate of the mixture. The initial concentration of F atoms is estimated at $\sim 1\times 10^{13}$ molecule cm^{-3}, based on a 30% dissociation efficiency for F_2. Under these conditions we estimate an OH formation time of $\sim 300\ \mu s$ ($k_6 = 1.1\times 10^{-11}$ cm^3 molecule^{-1} s^{-1}) [23] and an OH vibrational relaxation time faster than $\sim 400\ \mu s$ ($k_3 = 1.4\times 10^{-11}$ cm^3 molecule^{-1} s^{-1}),[24] considering only the gas phase relaxation by H_2O. These time scales are clearly much shorter than the OH residence time in the absorption cell and thus the OH rovibrational distribution is fully relaxed to a $v = 0$, near room temperature rotational distribution. It is worth stressing, however, that our analysis relies only on relative absorption or emission intensity measurements from a *common* initial state, and thus does not require the sample to be in any state of rotational equilibration, and makes no assumption regarding the rovibrational relaxation pathway or rates.

Figure 1(b) shows the configuration of the spectrometer during the absorption measurement. The light source used is a quartz halogen lamp. As in the emission work, a CaF_2 beam splitter is employed and the light is detected with a liquid nitrogen cooled InSb photodiode. A room temperature 2.5 μm long pass filter is used to eliminate high frequency IR source radiation. The White cell provides an absorption path length of 99.2 m. The limiting aperture diameter is 1.5 mm. The acquisition time is ~ 170 min. The spectrometer body is evacuated to minimize spurious absorptions in the same spectral region by the strong asymmetric stretch mode of water. The spectrum covers the $v = 1 \leftarrow 0$ absorption band, spanning the region from 3520 to 3900 cm^{-1}, with a resolution of 0.01 cm^{-1}.

In both the absorption and emission measurements the He (99.9% pure) buffer gas is passed through a trap containing molecular sieve material at liquid nitrogen temperature for further purification. For the emission experiments ozone is prepared by passing O_2 through an ac discharge and collecting the O_3 on silica gel maintained at dry ice temperature. The ozone is $\sim 90\%$ pure with the major impurity being O_2. The hydrogen gas ($> 99.9\%$ pure) is diluted in He to 4% concentrations and used without purification. For the absorption experiment a commercial mix of 5% F_2 in He was used directly from the cylinder.

III. RELATIVE INTENSITY RESULTS

OH spectra are produced by Fourier transforming the time domain interferograms which are directly measured. Each emission interferogram is zero filled to double its apparent resolution and then transformed to the frequency domain using a Hamming apodization function. Similarly, the absorption interferogram is zero filled to improve the apparent spectral resolution from 0.01 to 0.0065 cm^{-1} and Fourier transformed using a boxcar apodization function. Both the OH emission and absorption spectra must be corrected to account for frequency responsivity of the spectrometer, and furthermore, the OH emission spectra require correction for background blackbody radiation. This is accomplished as follows. For each data scan covering a given spectral region, two calibration scans are acquired. The first is a

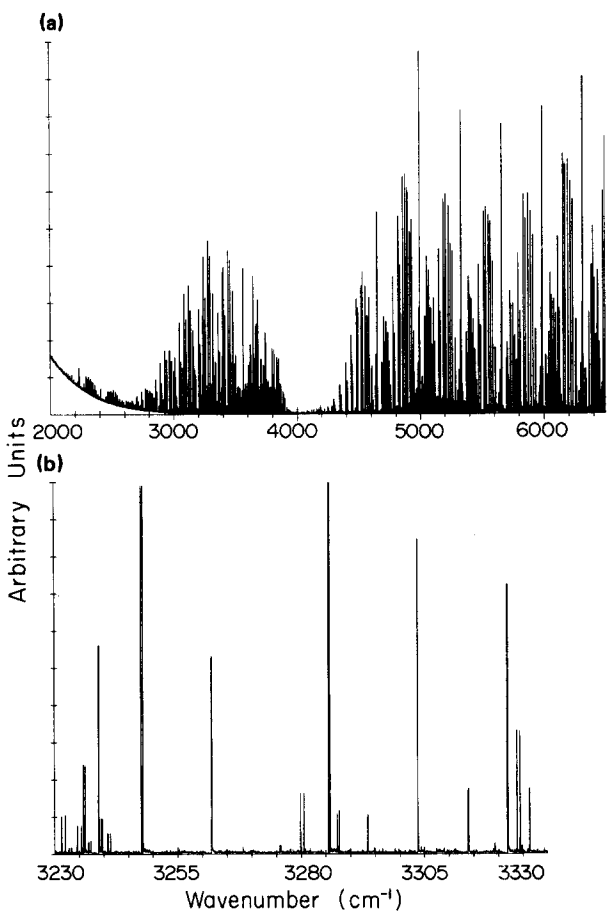

FIG. 2. (a) Low resolution plot of the OH infrared emission observed from the H + O_3 source, (b) Expanded plot of the spectrum in (a) illustrating the resolved rotational structure and signal to noise of the OH emission.

background scan taken with the ozone flow to the emission cell turned off, but with all other conditions left unchanged (including the H_2/He discharge). The background spectrum is subtracted from the OH spectrum to eliminate the background blackbody emission. This is a significant correction only for the $v = 9 \rightarrow 8$ and $v = 8 \rightarrow 7$ spectra since they occur at the lowest emission frequencies, but in any event does not affect the rovibrational measurement of any of the transition intensities since it constitutes only a baseline shift. The second calibration scan is a blackbody spectrum which is acquired by placing a calibrated blackbody source ($T \sim 880$ K) within the partially disassembled emission cell. In this way the blackbody radiation passes through each of the optical elements that the OH radiation traversed. The experimental blackbody spectrum is ratioed to a theoretical spectrum to yield the instrument response function. The background corrected OH spectrum is then divided by the instrument response function to provide the responsivity corrected spectrum from which relative intensities are determined. We have also tested this instrument response function using a lower temperature blackbody source and the calibrations agree near the peak emission frequencies to better than 2%–3%. Due to the decreased blackbody emission at increasing frequencies, however, the 880 K blackbody source emits sufficient radiation to calibrate the detector responsivity to better than 10% only for frequencies $\leqslant 6000$ cm^{-1}. For this reason no measurement of transition intensities in the lowest overtone series ($v = 2 \rightarrow 0, \nu_0 = 6970$ cm^{-1}) are reported. The measurements made in $v = 3 \rightarrow 1$ ($\nu_0 = 6640$ cm^{-1}) are estimated to be 40% uncertain whereas those made in $v = 4 \rightarrow 2$ ($\nu_0 = 6310\,cm^{-1}$) are estimated to be 25% uncertain based on the signal-to-noise ratio of the blackbody emission. The OH transitions were identified using the reported energy levels of Coxon and Foster.[25] We have checked our frequency calibration against N_2O ($00^01 \leftarrow 00^00$) frequencies of Guelachvili and Rao[26] and against the precise OH $v = 1 \leftarrow 0$ measurements of Amano[27] and estimate our measurements to be accurate to about 0.001 cm^{-1} for strong transitions.

The relative intensities reported in this work were obtained by integrating individual line strengths in the corrected spectra and taking the appropriate ratios. The area under each resonance was integrated by computer with an interactively chosen floating baseline. The reproducibility of the integration process is limited to better than a few percent by signal to noise. To eliminate the effects of variations in conditions from run to run, only ratios between transitions observed within a single spectrum measurement are used. The reported relative intensities are thus the averages of several independent observations from a series of nearly identical runs.

The observed intensity ratios are listed in Tables II–IV along with their uncertainties. The reported uncertainties, significant since the squares of their inverses are used to weight the fit to $\mu(r)$, are arrived at as follows. For each ratio the uncertainty due to random errors is estimated using 95% confidence limits. In addition to the random errors there are undoubtedly some small systematic errors in the measured relative emission intensities: We conservatively estimate

TABLE II. Ratio of $\Delta v = 1$ Einstein A coefficients[a] measured by FTIR emission.

v'	J'	F	Experimental ratio[b]	Ratio calculated from $\mu(r)$
1	3.5	1	2.85(0.77)	3.14
1	4.5	1	4.55(0.59)	3.60
1	5.5	1	5.81(0.70)	4.39
1	6.5	1	7.10(0.78)	5.61
1	7.5	1	13.60(13.60)	7.49
1	1.5	2	3.42(0.55)	2.89
1	2.5	2	3.21(0.35)	2.91
1	3.5	2	4.04(0.48)	3.39
1	4.5	2	4.72(0.61)	4.18
1	5.5	2	7.42(5.34)	5.36
1	6.5	2	5.29(5.29)	7.17
2	2.5	1	3.72(0.45)	3.62
2	3.5	1	3.87(0.62)	3.69
2	4.5	1	5.18(0.83)	4.46
2	5.5	1	5.87(1.41)	5.80
2	1.5	2	3.36(0.50)	3.14
2	2.5	2	3.88(0.66)	3.33
2	3.5	2	3.54(0.42)	4.10
2	4.5	2	7.59(1.67)	5.39
2	5.5	2	10.79(6.04)	7.50
3	2.5	1	4.86(1.02)	4.33
3	3.5	1	5.34(1.01)	4.76
3	4.5	1	7.10(1.28)	6.31
3	5.5	1	9.60(2.88)	9.28
3	6.5	1	15.90(15.90)	15.27
3	1.5	2	3.90(0.47)	3.60
3	2.5	2	4.90(1.37)	4.12
3	3.5	2	6.45(1.10)	5.56
3	4.5	2	9.50(3.23)	8.23
4	2.5	1	6.15(0.68)	5.97
4	3.5	1	7.89(1.03)	7.63
4	4.5	1	14.65(1.90)	12.46
4	5.5	1	22.20(10.88)	25.41
4	1.5	2	5.42(0.92)	4.55
4	2.5	2	6.79(0.88)	6.04
4	3.5	2	8.73(0.87)	9.94
5	2.5	1	12.30(1.85)	12.75
5	3.5	1	23.10(4.85)	26.79
5	4.5	1	$\geqslant$50.(100.)[c]	130.
5	1.5	2	7.50(1.57)	7.73
5	2.5	2	12.70(2.67)	15.60
6	2.5	1	$\geqslant$40.(80.)[c]	1410.
6	3.5	1	$\geqslant$40.(80.)[c]	31.
6	4.5	1	23.30(23.30)	9.82
6	5.5	1	4.81(1.83)	5.02
6	6.5	1	3.23(1.23)	3.14
6	7.5	1	2.29(0.87)	2.19
6	8.5	1	1.40(0.53)	1.62
6	9.5	1	1.37(1.37)	1.25
6	1.5	2	$\geqslant$20.(40.)[c]	138.
6	2.5	2	$\geqslant$20.(40.)[c]	105.
6	3.5	2	10.70(10.70)	14.86
6	4.5	2	4.10(4.10)	6.21
6	5.5	2	2.30(1.40)	3.57
6	6.5	2	2.10(1.28)	2.38
6	7.5	2	2.10(2.10)	1.72
7	2.5	1	0.36(0.16)	0.36
7	3.5	1	0.44(0.19)	0.36
7	4.5	1	0.38(0.17)	0.35
7	5.5	1	0.58(0.26)	0.34
7	1.5	2	0.34(0.22)	0.28
7	2.5	2	0.52(0.32)	0.35
9[d]	2.5	1	0.49(0.10)	0.49
9	3.5	1	0.28(0.06)	0.24
9	4.5	1	0.20(0.04)	0.14

TABLE II. (*continued*).

v'	J'	F	Experimental ratio[b]	Ratio calculated from $\mu(r)$
9	5.5	1	0.07(0.07)	0.08
9	1.5	2	0.64(0.36)	0.67
9	2.5	2	0.41(0.23)	0.32
9	3.5	2	0.26(0.15)	0.17
9	4.5	2	0.15(0.15)	0.10

[a] P branch A coefficient divided by R branch A coefficient.
[b] The number in parentheses is the calculated uncertainty for 95% confidence limits.
[c] For these measurements the R branch transition is too weak to be observed; the reported ratio is a lower limit.
[d] Transitions from $v' = 8 \rightarrow 7$ are too weak to be reliably reported due to a combination of small populations and low Einstein A coefficients.

TABLE IV. Ratio of $v = 1 \leftarrow 0$ Einstein A coefficients[a] measured in absorption.

J''	F	Experimental ratio[b]	Experimental ratio[c]	Ratio calculated from $\mu(r)$
2.5	1	2.12(32)[d]	2.08(20)[d]	2.17
3.5	1	2.92(44)	2.86(22)	2.95
4.5	1	3.95(79)	3.99(26)	3.80
5.5	1	5.2(16)	4.91(38)	4.99
6.5	1	···	8.3(19)	6.78
1.5	2	2.81(42)	2.45(15)	2.82
2.5	2	3.00(45)	2.73(17)	3.11
3.5	2	3.23(81)	3.92(38)	3.79
4.5	2	5.9(24)	4.61(47)	4.88

[a] P branch A coefficient divided by R branch A coefficient.
[b] Measured in this work by FTIR absorption.
[c] Measured in Ref. 5 by flash kinetic absorption methods.
[d] Uncertainties represent 95% confidence limits.

these to be less than 10% and report total uncertainties that are the convolution of the random and systematic error estimates. Ratios involving the $v = 4 \rightarrow 2$ band and the $v = 3 \rightarrow 1$ band are estimated to have larger systematic uncertainties (25% and 40%, respectively) because of the aforementioned difficulty of calibrating the spectrometer frequency response above 6000 cm^{-1} with a 880 K blackbody source. Emission intensity ratios that are observed only in a single run are reported to be 100% uncertain since these involve the measurement of at least one very weak transition which is unobserved in other scans. Some transitions are so weak that they are not observed within our S/N. In these cases, we report only a lower or upper limit to the corresponding P/R branch ratio. The Fourier transform $v = 1 \leftarrow 0$ absorption intensity ratios are each single measurements whose uncertainties are estimated from the high signal-to-noise ratio of the individual transitions.

Several control experiments have been carried out to minimize the possibility of systematic errors in the data: (1) To rule out the possibility of OH self-absorption affecting these results additional scans of the $v = 1 \rightarrow 0$ and $2 \rightarrow 1$ bands have been taken with the ozone flow to the emission cell reduced to produce only 50% of the normal OH concentrations. The ratios obtained in this scan agree to better than 1% with those found under optimum conditions; (2) The spectrometer response has been tested as a function of IR frequency by doing a second calibration in the $\Delta v = 1$ region with the blackbody set at a very different temperature ($T = 500$ K). As mentioned previously, the instrument response functions from the two calibrations agreed within 2%–3% over this spectral region; (3) The intensity ratios have also been measured as a function of spectrometer frequency resolution. The $v = 3 \rightarrow 2$ band was scanned with a resolution of 0.025 cm^{-1}, and transformed with resolutions of 0.025, 0.03, 0.04, and 0.05 cm^{-1}. The measured ratios were observed to be independent of resolution and apodization function over this range to within experimental uncertainties ($\sim 2\%$).

TABLE III. Ratio of $(\Delta v = 1)/(\Delta v = 2)$ Einstein A coefficients.[a]

v'	J	Experimental ratio	Ratio calculated from $\mu(r)$
9	1.5	0.18(4)[b]	0.18
9	2.5	0.19(5)	0.18
8	1.5	0.050(12)	0.056
8	2.5	0.061(15)	0.057
7	1.5	$\leqslant$0.009(18)[c]	0.004
6	1.5	$\leqslant$0.014(28)[c]	0.012
5	1.5	0.067(18)	0.088
4	1.5	0.24(8)	0.27
4	2.5	0.24(8)	0.27
3	1.5	0.53(27)	0.70

[a] Ratio of $\Delta v = 1$, $F = 1$ Q branch A factor over $\Delta v = 2$, $F = 1$ Q branch A factor, measured by FTIR emission.
[b] Uncertainties represent 95% confidence limits.
[c] For these measurements the $\Delta v = 1$ transition is too weak to be observed; the reported ratio is an upper limit.

IV. OH DIPOLE MOMENT FUNCTION AND EINSTEIN *A* FACTORS

The extraction of the OH dipole moment function from the measured ratios of Einstein A coefficients is performed using a procedure described elsewhere.[17] This procedure takes full account of and indeed is based upon the strong J dependence of the Einstein A factors induced by rotation–vibration interaction and by spin uncoupling. We express $\mu(r)$ in a polynomial expansion about the equilibrium bond length r_e

$$\mu(r) = \sum_i M_i (r - r_e)^i. \tag{8}$$

For a given trial $\mu(r)$, we can efficiently calculate all relevant Einstein A coefficients, and thus their ratios, from the following expression:

$$A = (16\pi^3\nu^3/3\epsilon_0 hc^3) \sum_{M''} |\langle v'',F'',J'',M''| \times \mu(r)|v',F',J',M'\rangle|^2, \quad (9)$$

where ν is the frequency of the transition (in Hz) and all other quantities are expressed in SI units. The state labels describe vibration (v), spin–orbit component (F), total angular momentum excluding nuclear spin (J), and the projection of J on a space fixed axis (M). We also calculate the OH permanent dipole moments in $v = 0$, 1, and 2 as the corresponding matrix elements in Eq. (9) which are diagonal in v. The wave functions used to obtain the appropriate matrix elements are based on the OH RKR potential presented previously.[17] The calculated intensity ratios and dipole moments are compared with the measured intensity ratios and dipole moments; the trial $\mu(r)$ is modified to minimize these discrepancies in a least-squares sense.

There are three types of data employed in the least-squares fits to $\mu(r)$. The first type of data consists of the J dependent ratios of P branch to R branch Einstein A coefficients within a given $\Delta v = 1$ vibrational band. The bulk of the data used in this work falls in this category. These ratios have a very strong J dependence which arises from rotation–vibration interaction and spin uncoupling. Rotation–vibration interaction causes a small amount of the permanent dipole moment to be added to (or subtracted from) the transition dipole moment of the nonrotating molecule for P (R) branch transitions. Since the permanent dipole moment (~ 1.7 D) is so large compared to typical transition dipole moments ($\sim \pm 0.01$ to ± 0.03 D), even a modest amount of rotation can lead to destructive cancellation of the transition moment, and thus dramatic changes in the observed intensity for some value of J in either the P or R branch. In essence, the method relies on measuring a pure vibrational transition moment by J dependent intensity effects resulting from a very well known permanent dipole moment. For low vibrations, these measurements are predominantly sensitive to M_1, the slope of $\mu(r)$ at r_e [see Eq. (8)]. For higher vibrations these data are sensitive to some linear combination of M_1, M_2, and M_3.

The second data set is made up of intensity ratios for $\Delta v = 1$ to $\Delta v = 2$ transitions which originate from a common upper state. The transitions used here are low J, Q branch transitions which are insensitive ($< 1\%$) to rotation–vibration interaction effects. These ratios are mainly sensitive to r_m, the position of the maximum of the dipole moment function. This follows because the wave functions for *low* vibrational quantum numbers sample predominantly internuclear separations on the *rising* side of $\mu(r)$ (i.e., $r < r_m$) which yields a *positive* $\Delta v = 1$ transition moment. Conversely, due to anharmonicity, the wave functions for *high* vibrational quanta sample predominantly the *falling* side of $\mu(r)$ (i.e., $r > r_m$), which leads to a *negative* $\Delta v = 1$ transition moment. For some intermediate value of v the vibrational wave function is approximately centered with respect to r_m, and thus the $\Delta v = 1$ transition moment nearly vanishes. Since the $\Delta v = 2$ intensities depend on the *curvature* in $\mu(r)$ and are thus relatively independent of v, a "notch" exists in the $\Delta v = 1/\Delta v = 2$ ratios at some number of vibrational quanta, thus providing an extremely sensitive probe of r_m.

TABLE V. Experimentally measured dipole moment for OH.

	Experimental dipole moment (D)[a]	Dipole moment calculated from $\mu(r)$
$\mu(v=0)$	1.655 20(10)[b]	1.655 19
$\mu(v=1)$	1.662 57(16)	1.662 53
$\mu(v=2)$	1.664 8(10)	1.666 3
$\mu(v=1)-\mu(v=0)$	0.007 35(7)	0.007 34

[a] Taken from Ref. 16.
[b] Uncertainties represent 95% confidence limits.

The third data set consists of the permanent dipole moment measurements of OH in $v = 0,1$ and 2 reported by Peterson *et al.*[16] The $v = 0$ dipole moment sets the scale of $\mu(r)$. The vibrational dependence of the dipole moment is also sensitive to r_m. This follows since the permanent dipole moment for the lower vibrational states, which is simply the expectation values of $\mu(r)$, increases slowly with v. However, this trend must reverse in higher vibrational states whose wave functions have significant amplitude at $r > r_m$ values where $\mu(r)$ is decreasing rapidly.

To determine $\mu(r)$ we perform a nonlinear weighted least-squares fit to the data sets discussed above and presented in Tables II–V. The weight used for each quantity is the inverse square of its reported uncertainty. The polynomial expansion is truncated after the cubic term, and fitted to determine four quantities (M_0, M_1, M_2, M_3) from 100 experimental measurements [87 $\Delta v = 1$ $P(J)/R(J)$ relative intensities, 10 $\Delta v = 1$, $Q(J)/\Delta v = 2$, $Q(J)$ relative intensities and three dipole moments].

The results of the fit are shown in Tables VI and VII. In Table VI the values of the M_i are presented with our estimated 95% confidence limits which are intended to account for both random and potential systematic errors in $\mu(r)$. In Table VII the correlation matrix from the fit is reproduced showing little correlation between the M_i, M_0 is determined with high precision due to the extremely precise permanent dipole moment data. The uncertainties of the M_i are arrived at as follows. The M_0 uncertainty is taken as the 95% uncertainty estimated by the fitting procedure. The uncertainties in the M_i ($i = 1,2,3$) are reported as the convolution of the

TABLE VI. Polynomial expansion coefficients of $\mu(r)$ for OH.[a]

Coefficient	Present results	Previous results[c]
M_0	1.6502(2)[b] D	1.6498(6) D
M_1	0.538(29)[c] D/Å	0.561(32) D/Å
M_2	−0.796(51) D/Å^2	−0.75(17) D/Å^2
M_3	−0.739(50) D/Å^3	−1.5(11) D/Å^3

[a] $\mu(r) = \Sigma_i M_i (r - r_e)^i$.
[b] Numbers in parentheses represent 95% confidence limits.
[c] From Ref. 5 of Nelson *et al.* We note here that Table IV of Ref. 5 has a typographical error in M_1 and M_2. The correct values however, are stated elsewhere throughout the previous paper and used for all calculations reported therein.

TABLE VII. Correlation matrix from fit to determine $\mu(r)$.[a]

	M_0	M_1	M_2	M_3
M_0	1			
M_1	−0.13	1		
M_2	−0.01	−0.93	1	
M_3	0.24	−0.20	−0.49	1

[a] $\mu(r) = \Sigma_i M_i (r - r_e)^i$.

fitting uncertainty with a systematic 5% uncertainty. The extra 5% uncertainty is somewhat arbitrary, but intended to account conservatively for the fact that the dipole moment function is represented only approximately as a cubic polynomial over the range of internuclear separation of interest. For the calculation of $\Delta v = 1$, 2, and 3 transition intensities with $v' \leqslant 9$ (which requires knowledge of $\mu(r)$ between 0.70 and 1.76 Å), the cubic polynomial limitation is not a serious problem. We have tested this by comparing calculations of Einstein A coefficients from cubic polynomial and quintic polynomial representations of the *ab initio* $\mu(r)$ of Langhoff *et al.*[14] Typically, the Einstein A coefficients differ only by a few per cent using the cubic representation. For weak transitions and $\Delta v = 1$ transitions from high v levels however, the discrepancies can be considerably larger (10%–30%), but always within the uncertainties implied by 5% systematic uncertainties on the M_i. As a further test of our cubic representation of $\mu(r)$, we have also carried out least-squares fits including quartic terms. These fits yield only a small quartic term (-0.18 D/Å^4) with uncertainties that include zero. This indicates that $\Delta v = 1$ and $\Delta v = 2$ Einstein A factors consistent with our data can be calculated accurately with a cubic $\mu(r)$ and that the data neither require nor justify a higher order representation of $\mu(r)$.

It is worth noting that the large body of measurements fitted in this work provides the luxury of data redundancy. We can perform fits to $\mu(r)$ which delete large subportions of the data and observe the effect on $\mu(r)$. For example, if we delete all of the $\Delta v = 1$ emission data (70 measurements) and fit $\mu(r)$ solely to the $v = 1 \leftarrow 0$ absorption P/R ratios, the permanent dipole moments and the $\Delta v = 1/\Delta v = 2$ emission ratios (30 measurements), we still obtain a dipole moment function which agrees with the reported function within our reported uncertainties. Several tests of this type are shown in Table VIII. The other tests include fits to $\mu(r)$ which exclude the $v = 1 \leftarrow 0$ absorption measurements, the $\Delta v = 1/\Delta v = 2$ Q branch ratios and the vibrational dependence of the dipole moments. The excellent agreement between the partial fits and the fit to the total data set provides strong evidence that the reported dipole moment function is free of significant systematic error.

Given the extreme importance of the OH radiative rates, as well as the sophisticated methods required to determine these rates from the dipole moment function, we have used our experimentally determined $\mu(r)$ to calculate Einstein A factors from Eq. (9)[17] for transitions with $\Delta v = 1$–3, $v' < 10$, $\Delta J = 0, \pm 1$, $J < 14.5$, and $F = 1,2$. In order to facilitate the use of these experimental OH radiative rates the $\Delta v = 1,2$, and 3 transition intensities are explicitly presented in Tables IX, X, and XI, respectively. [In the interest of space, only the values for the predominantly thermally populated $J \leqslant 5.5$ are reported herein; the complete tables up to $J \leqslant 14.5$ are readily available from the Physics Auxiliary Publication Service (PAPS)[28] or from the authors upon request.] The uncertainties reported in these Tables are the result of propagating the uncertainties of the M_i values independently and represent our best assessment of 95% confidence limits. Since $\mu(r)$ is not expected to be trustworthy outside the region bordered by the OH $v = 9$ classical turning points, we report no Einstein A coefficients involving states with $v \geqslant 10$. Similarly, we do not present Einstein A coefficients for the high overtone transitions with $\Delta v \geqslant 4$. These transitions are generally very weak and potentially quite sensitive to small quartic higher terms in the dipole moment function which have been neglected in the present analysis. However, given the quality and magnitude of data on the $\Delta v = 1,2$ transitions, it would require only a few absolute measurements of the $\Delta v = 3,4$ overtone transitions to extend the dipole moment expansion out to even higher order.

V. DISCUSSION

In Tables II–IV the predicted values of the experimental observables from the fit are listed with the experimental

TABLE VIII. Polynomial expansion coefficients of $\mu(r)$[a] from fits to subsets of all data.

	M_0	M_1	M_2	M_3
All data included	1.6502(2)D	0.54(3)D/Å	−0.80(5)D/Å^2	−0.74(5)D/Å^3
Subset of data excluded				
$v = 1 \leftarrow 0$ absorption[b]	1.6502D	0.53D/Å	−0.76D/Å^2	−0.75D/Å^3
$\Delta v = 1$ emission[c]	1.6501D	0.56D/Å	−0.85D/Å^2	−0.75D/Å^3
$\Delta v = 1/\Delta v = 2$[d]	1.6502D	0.54D/Å	−0.79D/Å^2	−0.74D/Å^3
μ for $v = 1,2$[e]	1.6500D	0.53D/Å	−0.75D/Å^2	−0.80D/Å^3

[a] $\mu(r) = \Sigma_i M_i (r - r_e)^i$.
[b] Fit to 83 data points excluding the P/R ratios measured in absorption for the $v = 1 \leftarrow 0$ band.
[c] Fit to 30 data points excluding the P/R ratios measured in emission for $\Delta v = 1$ bands with $v' < 10$.
[d] Fit to 90 data points excluding the $\Delta v = 1/\Delta v = 2$ Q branch ratios.
[e] Fit to 98 data points excluding the permanent dipole moment measurements in $v = 1$ and $v = 2$.

TABLE IX. Einstein A coefficients for $\Delta v = 1$ transitions (Hz).[a,b]

v''	v'	J''	$P1$	$Q1$	$R1$	$P2$	$Q2$	$R2$
0	1	0.5	···	···	···	···	5.29(64)	4.2(6)
0	1	1.5	···	9.14(111)	3.2(5)	12.2(13)	1.18(14)	4.3(7)
0	1	2.5	8.1(8)	3.69(45)	3.7(6)	12.1(12)	0.58(7)	3.9(7)
0	1	3.5	10.4(10)	1.92(24)	3.5(6)	12.6(12)	0.37(4)	3.3(6)
0	1	4.5	11.7(11)	1.14(14)	3.1(6)	13.2(12)	0.26(3)	2.7(6)
0	1	5.5	12.7(11)	0.74(9)	2.5(6)	13.9(12)	0.20(2)	2.1(5)
1	2	0.5	···	···	···	···	7.02(100)	5.4(9)
1	2	1.5	···	12.15(174)	4.0(7)	16.7(21)	1.55(22)	5.3(10)
1	2	2.5	11.1(13)	4.91(71)	4.5(9)	16.8(20)	0.75(11)	4.6(10)
1	2	3.5	14.5(17)	2.56(37)	4.1(9)	17.7(20)	0.47(7)	3.7(9)
1	2	4.5	16.5(18)	1.52(22)	3.3(8)	18.8(20)	0.34(5)	2.8(8)
1	2	5.5	18.1(19)	0.99(14)	2.6(8)	20.0(20)	0.25(4)	2.0(7)
2	3	0.5	···	···	···	···	6.34(113)	4.5(10)
2	3	1.5	···	11.01(197)	3.3(8)	15.8(24)	1.39(25)	4.3(10)
2	3	2.5	10.7(16)	4.45(80)	3.5(9)	16.4(23)	0.67(12)	3.4(10)
2	3	3.5	14.2(19)	2.32(42)	2.9(9)	17.6(23)	0.42(8)	2.5(9)
2	3	4.5	16.5(21)	1.38(25)	2.1(8)	18.9(23)	0.29(5)	1.6(7)
2	3	5.5	18.3(22)	0.89(16)	1.4(7)	20.3(24)	0.22(4)	0.9(5)
3	4	0.5	···	···	···	···	4.35(16)	2.8(9)
3	4	1.5	···	7.56(184)	1.9(6)	11.8(24)	0.94(23)	2.3(9)
3	4	2.5	8.2(15)	3.06(75)	1.7(7)	12.6(23)	0.45(11)	1.5(7)
3	4	3.5	11.2(20)	1.59(39)	1.2(6)	14.0(23)	0.28(7)	0.8(6)
3	4	4.5	13.2(22)	0.94(23)	0.7(5)	15.5(24)	0.19(5)	0.3(4)
3	4	5.5	15.0(23)	0.60(15)	0.2(3)	16.9(25)	0.14(4)	0.0(1)
4	5	0.5	···	···	···	···	2.04(80)	1.0(6)
4	5	1.5	···	3.55(140)	0.5(4)	6.5(20)	0.44(17)	0.6(5)
4	5	2.5	4.8(13)	1.43(57)	0.3(3)	7.6(20)	0.20(8)	0.2(3)
4	5	3.5	6.9(17)	0.74(30)	0.1(2)	8.8(21)	0.12(5)	0.0(1)
4	5	4.5	8.5(19)	0.43(18)	0.0(1)	10.2(22)	0.08(4)	0.1(2)
4	5	5.5	10.1(21)	0.27(11)	0.2(3)	11.6(23)	0.06(3)	0.6(5)
5	6	0.5	···	···	···	···	0.36(37)	0.0(1)
5	6	1.5	···	0.62(64)	0.0(1)	2.0(12)	0.07(8)	0.0(1)
5	6	2.5	1.7(9)	0.24(26)	0.1(2)	2.9(13)	0.03(4)	0.3(4)
5	6	3.5	2.8(12)	0.12(13)	0.5(5)	3.9(15)	0.02(2)	1.0(7)
5	6	4.5	3.9(14)	0.07(8)	1.2(8)	4.9(16)	0.01(1)	2.0(11)
5	6	5.5	5.0(16)	0.04(5)	2.3(11)	6.0(18)	0.01(1)	3.4(14)
6	7	0.5	···	···	···	···	0.14(25)	0.7(6)
6	7	1.5	···	0.25(44)	0.9(6)	0.0(1)	0.03(6)	1.6(10)
6	7	2.5	0.1(2)	0.11(19)	2.0(10)	0.2(4)	0.02(3)	2.9(14)
6	7	3.5	0.3(4)	0.07(11)	3.4(14)	0.6(6)	0.01(2)	4.7(18)
6	7	4.5	0.7(7)	0.05(7)	5.2(18)	1.1(8)	0.01(1)	6.8(22)
6	7	5.5	1.2(9)	0.04(5)	7.4(22)	1.6(10)	0.01(1)	9.5(26)
7	8	0.5	···	···	···	···	2.12(106)	3.7(14)
7	8	1.5	···	3.75(187)	3.7(13)	2.0(14)	0.47(23)	6.1(20)
7	8	2.5	0.8(7)	1.58(78)	6.6(20)	1.0(9)	0.23(11)	8.8(25)
7	8	3.5	0.5(6)	0.87(42)	9.4(26)	0.4(6)	0.15(7)	11.8(30)
7	8	4.5	0.2(4)	0.55(26)	12.5(31)	0.1(3)	0.11(5)	15.4(35)
7	8	5.5	0.0(2)	0.38(18)	16.1(36)	0.0(1)	0.09(4)	19.4(40)
8	9	0.5	···	···	···	···	6.87(206)	9.5(24)
8	9	1.5	···	12.13(363)	8.9(22)	9.2(33)	1.48(44)	14.1(33)
8	9	2.5	4.7(18)	5.10(152)	14.3(32)	6.3(26)	0.71(21)	18.4(39)
8	9	3.5	4.3(19)	2.77(82)	19.0(39)	4.5(21)	0.45(13)	23.0(45)
8	9	4.5	3.5(17)	1.73(50)	23.8(46)	3.2(17)	0.32(9)	27.9(51)
8	9	5.5	2.6(15)	1.18(34)	28.9(52)	2.3(14)	0.26(7)	33.4(57)

[a] Numbers in parentheses represent 95% confidence limits, or in cases of vanishingly weak transitions, an estimate of an upper limit on radiative rate.
[b] A complete version of this table up to $J'' \leqslant 14.5$ can be obtained by request from the Physics Auxiliary Publication Service (PAPS) or by writing to the authors (see Ref. 28).

data. The agreement in almost all cases is excellent, however, there are two notable exceptions. First of all, the $v = 2$ dipole moment determined from microwave studies (see Table V) is not reproduced within its reported uncertainty, and therefore seems to be inconsistent with the observed $\Delta v = 1/\Delta v = 2$ intensity ratios. Other authors have also expressed concern over the reported $v = 2$ dipole moment.[10,15] Removal of the $v = 2$ dipole moment from the fit, however, changes the M_i negligibly ($< 0.5\%$), and therefore it has been retained. The other measurements which seem to display systematic deviations are the $v = 1 \rightarrow 0$ P/R emission intensity ratios (see Table II). These ratios appear to be sys-

TABLE X. Einstein A coefficients for $\Delta v = 2$ transitions (Hz).[a,b]

v''	v'	J''	$P1$	$Q1$	$R1$	$P2$	$Q2$	$R2$
0	2	0.5	...	...	...	...	3.40(28)	3.1(3)
0	2	1.5	...	5.88(48)	2.5(2)	7.0(5)	0.76(6)	3.6(3)
0	2	2.5	4.4(3)	2.38(19)	3.2(3)	6.5(5)	0.37(3)	3.7(3)
0	2	3.5	5.4(4)	1.25(10)	3.5(3)	6.4(5)	0.24(2)	3.6(3)
0	2	4.5	5.8(4)	0.75(6)	3.5(3)	6.4(5)	0.17(1)	3.5(3)
0	2	5.5	6.1(4)	0.49(4)	3.4(3)	6.5(4)	0.13(1)	3.4(3)
1	3	0.5	...	...	...	...	9.05(71)	8.3(7)
1	3	1.5	...	15.70(123)	6.7(6)	18.6(14)	2.01(16)	9.5(8)
1	3	2.5	11.8(9)	6.39(50)	8.6(7)	17.4(13)	0.98(8)	9.7(9)
1	3	3.5	14.5(10)	3.35(26)	9.2(8)	17.1(12)	0.62(5)	9.6(9)
1	3	4.5	15.6(11)	2.01(16)	9.2(9)	17.2(12)	0.45(3)	9.3(9)
1	3	5.5	16.2(11)	1.32(10)	9.1(9)	17.3(12)	0.34(3)	8.9(9)
2	4	0.5	...	...	...	...	15.95(121)	14.6(12)
2	4	1.5	...	27.73(210)	11.7(10)	32.9(24)	3.51(27)	16.7(14)
2	4	2.5	20.9(15)	11.31(86)	15.0(13)	30.8(22)	1.71(13)	17.1(15)
2	4	3.5	25.6(18)	5.94(45)	16.0(14)	30.3(21)	1.08(8)	16.8(15)
2	4	4.5	27.6(19)	3.58(27)	16.1(14)	30.4(20)	0.77(6)	16.2(15)
2	4	5.5	28.8(19)	2.35(18)	15.8(15)	30.7(20)	0.59(4)	15.5(15)
3	5	0.5	...	...	...	...	23.15(171)	21.1(16)
3	5	1.5	...	40.33(298)	17.0(13)	48.0(34)	5.07(37)	24.2(19)
3	5	2.5	30.4(21)	16.49(122)	21.7(18)	44.9(31)	2.45(18)	24.6(21)
3	5	3.5	37.3(25)	8.68(64)	23.1(19)	44.3(29)	1.54(11)	24.1(21)
3	5	4.5	40.2(26)	5.23(39)	23.1(20)	44.4(29)	1.10(8)	23.3(21)
3	5	5.5	42.0(27)	3.44(25)	22.6(20)	44.9(28)	0.84(6)	22.1(21)
4	6	0.5	...	...	...	...	29.78(215)	27.1(21)
4	6	1.5	...	51.99(376)	21.7(17)	62.0(43)	6.48(47)	30.9(24)
4	6	2.5	39.3(27)	21.31(154)	27.6(22)	58.1(39)	3.10(22)	31.4(26)
4	6	3.5	48.2(32)	11.24(81)	29.3(24)	57.4(37)	1.94(14)	30.7(26)
4	6	4.5	52.1(34)	6.78(49)	29.3(25)	57.7(37)	1.38(10)	29.4(26)
4	6	5.5	54.5(34)	4.46(32)	28.4(25)	58.3(36)	1.05(8)	27.8(26)
5	7	0.5	...	...	...	...	35.02(249)	31.8(24)
5	7	1.5	...	61.27(436)	25.3(19)	73.4(50)	7.57(54)	36.1(28)
5	7	2.5	46.5(31)	25.17(179)	32.1(25)	68.8(45)	3.60(26)	36.5(29)
5	7	3.5	57.2(37)	13.30(95)	33.9(28)	68.1(44)	2.24(16)	35.4(30)
5	7	4.5	61.9(39)	8.03(57)	33.7(29)	68.6(43)	1.58(11)	33.8(30)
5	7	5.5	64.8(40)	5.28(38)	32.6(29)	69.4(42)	1.20(09)	31.8(29)
6	8	0.5	...	...	...	...	38.09(269)	34.4(26)
6	8	1.5	...	66.79(472)	27.2(21)	80.4(54)	8.18(58)	38.9(30)
6	8	2.5	50.9(34)	27.49(195)	34.4(27)	75.6(49)	3.86(27)	39.0(31)
6	8	3.5	62.8(40)	14.56(103)	36.1(30)	75.0(48)	2.38(17)	37.7(32)
6	8	4.5	68.1(43)	8.80(62)	35.7(30)	75.6(47)	1.68(12)	35.6(31)
6	8	5.5	71.5(44)	5.79(41)	34.2(30)	76.7(46)	1.27(9)	33.2(30)
7	9	0.5	...	...	...	...	38.31(272)	34.4(26)
7	9	1.5	...	67.32(478)	27.0(21)	81.6(55)	8.17(58)	38.5(30)
7	9	2.5	51.8(34)	27.76(197)	33.8(27)	77.1(50)	3.83(27)	38.3(31)
7	9	3.5	64.1(41)	14.72(105)	35.2(29)	76.7(49)	2.34(17)	36.6(31)
7	9	4.5	69.7(44)	8.90(63)	34.4(30)	77.5(48)	1.64(12)	34.2(31)
7	9	5.5	73.3(45)	5.85(42)	32.6(30)	78.8(48)	1.23(9)	31.5(30)

[a] Numbers in parentheses represent 95% confidence limits, or in cases of vanishingly weak transitions, an estimate of an upper limit on radiative rate.
[b] A complete version of this table up to $J'' = 14.5$ can be obtained by request from the Physics Auxiliary Publication Service (PAPS) or by writing to the authors (see Ref. 28).

tematically higher than those predicted from the fit (at the ~20% level), unlike the $v = 1 \leftarrow 0$ absorption ratios (see Table IV) which were obtained in two separate experiments. The $v = 1 \rightarrow 0$ emission bands are unique in that they fall in the region of strong fundamental water bands and may therefore be weakly but selectively attenuated by atmospheric pressure broadened absorptions in the spectrometer body. We emphasize that this discrepancy has only a small influence on $\mu(r)$. The complete removal of the $v = 1 \rightarrow 0$ emission data changes the M_i by 1% to 3% which is well within their reported uncertainties.

The significantly larger set of data available in this analysis allows a considerably more precise determination of $\mu(r)$ over an extended range of internuclear separation. The resulting dipole moment function falls well within the range of the uncertainties of the previous $\mu(r)$. For example, the M_0 and M_1 terms prove to be quite well determined previously; the reported values shift only slightly in this work and are not more precisely determined. However, the uncertainties accompanying the refined $\mu(r)$ are dramatically smaller for the higher order terms, i.e., the uncertainties in M_3 and M_2 are reduced 20- and 3-fold, respectively.

TABLE XI. Einstein A coefficients for $\Delta v = 3$ transitions (Hz).[a,b]

v''	v'	J''	$P1$	$Q1$	$R1$	$P2$	$Q2$	$R2$
0	3	1.5	...	...	...	...	0.37(4)	0.3(1)
0	3	1.5	...	0.64(7)	0.3(1)	0.8(1)	0.08(1)	0.4(1)
0	3	2.5	0.5(1)	0.26(3)	0.4(1)	0.7(1)	0.04(1)	0.4(1)
0	3	3.5	0.6(1)	0.14(2)	0.4(1)	0.7(1)	0.03(1)	0.4(1)
0	3	4.5	0.6(1)	0.08(1)	0.4(1)	0.7(1)	0.02(1)	0.4(1)
0	3	5.5	0.6(1)	0.05(1)	0.4(1)	0.7(1)	0.01(1)	0.4(1)
1	4	0.5	...	...	...	...	1.36(15)	1.3(1)
1	4	1.5	...	2.37(26)	1.0(1)	2.8(3)	0.30(3)	1.5(2)
1	4	2.5	1.7(2)	0.96(11)	1.3(2)	2.6(3)	0.15(2)	1.5(2)
1	4	3.5	2.1(2)	0.51(6)	1.4(2)	2.5(2)	0.09(1)	1.5(2)
1	4	4.5	2.3(2)	0.31(3)	1.5(2)	2.5(2)	0.07(1)	1.5(2)
1	4	5.5	2.4(2)	0.20(2)	1.5(2)	2.5(2)	0.05(1)	1.4(2)
2	5	0.5	...	...	...	...	3.11(32)	2.9(3)
2	5	1.5	...	5.42(56)	2.3(3)	6.3(6)	0.68(7)	3.4(4)
2	5	2.5	4.0(4)	2.21(23)	3.0(3)	5.9(6)	0.33(3)	3.5(4)
2	5	3.5	4.8(5)	1.17(12)	3.3(4)	5.7(5)	0.21(2)	3.5(4)
2	5	4.5	5.2(5)	0.70(7)	3.3(4)	5.7(5)	0.15(2)	3.4(4)
2	5	5.5	5.4(5)	0.46(5)	3.3(4)	5.7(5)	0.12(1)	3.3(4)
3	6	0.5	...	...	...	...	5.66(55)	5.3(5)
3	6	1.5	...	9.87(95)	4.3(4)	11.5(11)	1.24(12)	6.1(6)
3	6	2.5	7.2(7)	4.05(39)	5.5(6)	10.7(10)	0.60(6)	6.3(7)
3	6	3.5	8.8(8)	2.14(21)	6.0(7)	10.4(9)	0.37(4)	6.3(7)
3	6	4.5	9.4(8)	1.29(12)	6.1(7)	10.4(9)	0.27(3)	6.2(7)
3	6	5.5	9.8(8)	0.85(8)	6.0(7)	10.4(9)	0.21(2)	6.0(7)
4	7	0.5	...	...	...	...	8.96(81)	8.4(8)
4	7	1.5	...	15.66(142)	6.7(7)	18.3(16)	1.95(18)	9.7(10)
4	7	2.5	11.5(10)	6.43(58)	8.7(9)	16.9(14)	0.93(8)	10.0(10)
4	7	3.5	13.9(12)	3.40(31)	9.4(10)	16.5(14)	0.58(5)	10.0(10)
4	7	4.5	14.9(12)	2.06(19)	9.6(10)	16.4(13)	0.41(4)	9.8(11)
4	7	5.5	15.5(12)	1.36(12)	9.5(10)	16.5(13)	0.32(3)	9.5(11)
5	8	0.5	...	...	...	...	12.85(110)	12.0(11)
5	8	1.5	...	22.51(193)	9.6(9)	26.3(22)	2.77(24)	13.9(13)
5	8	2.5	16.5(13)	9.27(79)	12.5(12)	24.3(19)	1.32(11)	14.3(14)
5	8	3.5	20.0(16)	4.92(42)	13.4(13)	23.7(18)	0.82(7)	14.3(14)
5	8	4.5	21.4(16)	2.98(25)	13.7(14)	23.6(18)	0.58(5)	14.0(14)
5	8	5.5	22.2(17)	1.97(17)	13.5(14)	23.7(18)	0.44(4)	13.5(14)
6	9	0.5	...	...	...	...	17.05(138)	15.9(13)
6	9	1.5	...	29.94(242)	12.8(11)	35.0(27)	3.66(30)	18.4(16)
6	9	2.5	21.9(17)	12.36(100)	16.5(15)	32.4(24)	1.73(14)	19.0(17)
6	9	3.5	26.6(20)	6.57(53)	17.7(16)	31.6(23)	1.07(9)	18.8(17)
6	9	4.5	28.5(21)	3.99(32)	18.0(17)	31.5(23)	0.75(6)	18.4(18)
6	9	5.5	29.6(21)	2.64(21)	17.8(17)	31.6(22)	0.57(5)	17.7(18)

[a] Numbers in parentheses represent 95% confidence limits, or in cases of vanishingly weak transitions, an estimate of an upper limit on radiative rate.
[b] A complete version of this table up to $J'' \leqslant 14.5$ can be obtained by request from the Physics Auxiliary Publication Service (PAPS) or by writing to the authors (see Ref. 28).

The unique feature of our approach to the determination of $\mu(r)$ is the exploitation of the strong J dependence of the $\Delta v = 1$ vibrational transition strengths. The measurement of this effect in low v transitions provides a precise determination of M_1, the slope of $\mu(r)$ near r_e. This information is otherwise difficult to obtain. The $\Delta v = 1/\Delta v = 2$ ratios, for example, are not very sensitive to slope of $\mu(r)$ itself, but rather put a constraint on M_1, M_2, and M_3, such that the maximum of $\mu(r)$ occurs in the correct place. A fit of $\mu(r)$ solely to our $\Delta v = 1/\Delta v = 2$ ratios and the $v = 0$–2 dipole moments produces a dipole moment function whose slope is far too steep [0.71 D/Å as opposed to the reported value of 0.54(3)D/Å]. This reveals a serious potential difficulty in previous attempts to fit $\mu(r)$ to $\Delta v = 1/\Delta v = 2$ data which are relatively insensitive to its slope. With an accurate value of M_1 established from the analysis of the $\Delta v = 1$ P/R measurements, however, the $\Delta v = 1/\Delta v = 2$ ratios can determine the higher terms in $\mu(r)$ quite well.

In Fig. 3 we show the dipole moment function reported in this work (solid line) together with four other *ab initio* and empirical functions. In the lower panel is plotted the deviation of the four functions from the $\mu(r)$ reported here. The atmospherically important region of the function which lies between 0.70 and 1.76 Å (the $v = 9$ classical turning points) is displayed. The four functions include the theoretical functions of Langhoff, Werner, and Rosmus[14] (LWR), Langhoff, Bauschlicher, and Taylor[15] (LBT), Stevens *et al.*,[12] as well as the empirical dipole moment function of Turnbull and Lowe (TL).[10] The LWR function (chain dashed line) gives the best agreement with this work, differing mostly due to its ~5% smaller slope at r_e. This LWR function results from shifting a high level *ab initio* dipole

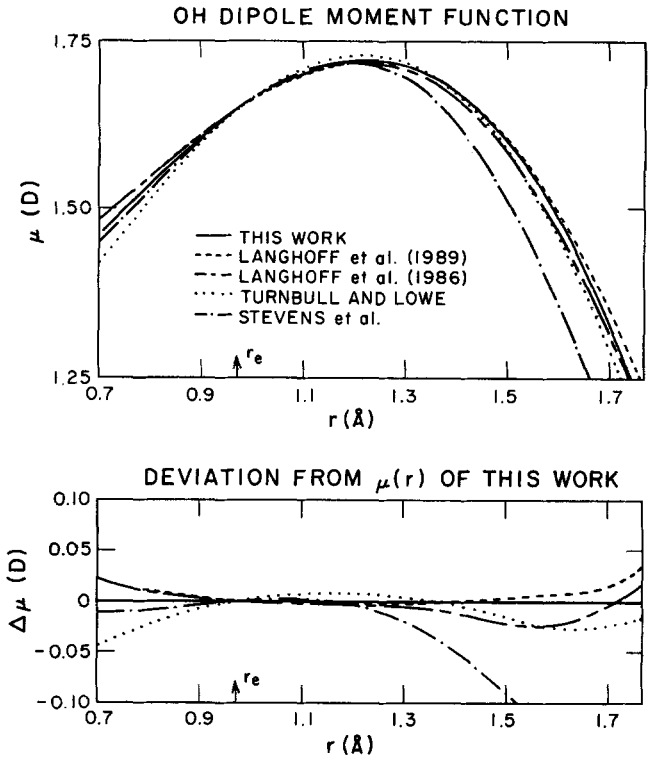

FIG. 3. Dipole moment function from this work (solid curve) compared with previously reported dipole moment functions.

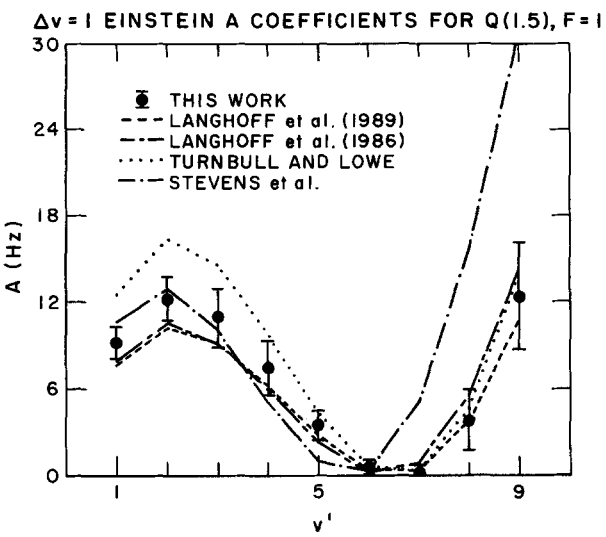

FIG. 4. Einstein A coefficients predicted by various dipole moment functions for $\Delta v = 1$ $Q(1.5)$, $F = 1$.

moment function by 0.03 bohr in order to match the experimentally measured increase in OH dipole moment between $v = 1$ and $v = 0$. The more recent LBT *ab initio* calculation (dashed line) is also in fairly good agreement with our present work, although its slope at r_e is even smaller. The scaled *ab initio* dipole moment function of Stevens *et al.* (chain dotted line) turns over at too small a value of r, and exhibits a somewhat too steep slope near r_e. Finally, the TL function (dotted line) is also too steep near r_e, although the larger r behavior of this function is in good agreement with the reported $\mu(r)$.

These differences between the various dipole moment functions are more sensitively reflected in the Einstein A coefficients which they imply. In Figs. 4–6, we plot the $\Delta v = 1$–3 Q(1.5), $F = 1$, Einstein A coefficients predicted by each of the dipole moment functions, with the experimental results of this work shown as solid circles with uncertainties. The $\Delta v = 1$ coefficients (Fig. 4) go through a sharp minimum in the $v' \sim 6$ region as mentioned previously. This occurs because the transition moment changes sign for the higher vibrational states which have more amplitude outside r_m than inside. Since the Stevens *et al.*[12] function has too small a value for r_m, it predicts the $v = 6 \rightarrow 5$ and $5 \rightarrow 4$ bands to have the least intensity at low J. The experimentally observed $\Delta v = 1/\Delta v = 2$ intensity ratios, on the other hand, demonstrate clearly that the minimum occurs between the $v = 7 \rightarrow 6$ and $6 \rightarrow 5$ bands. Similarly, the excess slope of the TL dipole moment function is reflected in the overly large A coefficients predicted for the $v = 1 \rightarrow 0$, $2 \rightarrow 1$ and $3 \rightarrow 2$ transitions.

A survey of Figs. 4–6 reveals that the LWR $\mu(r)$, which appears to be most similar to the reported $\mu(r)$, also produces Einstein A coefficients which are in agreement (i.e., within 20%–30%) with our experimental results. This is a remarkable achievement since previous experimental and theoretical measurements have been in disagreement by as much as 500%. (See Table XII.) Interestingly, the more

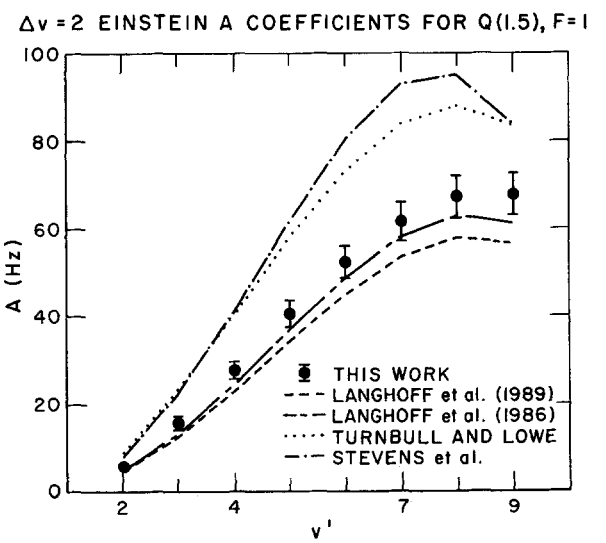

FIG. 5. Einstein A coefficients predicted by various dipole moment functions for $\Delta v = 2$ $Q(1.5)$, $F = 1$.

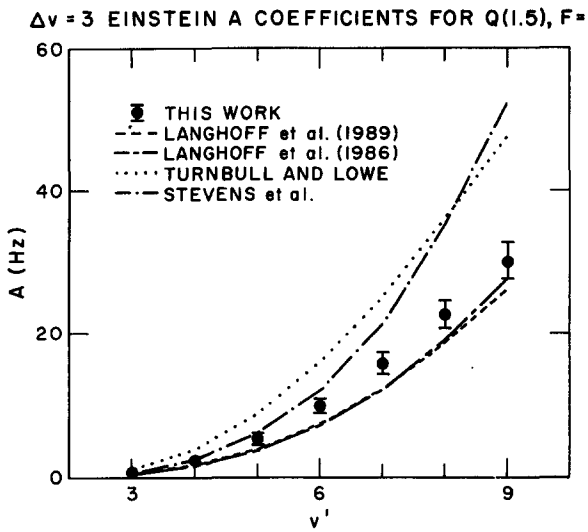

FIG. 6. Einstein A coefficients predicted by various dipole moment functions for $\Delta v = 3$ $Q(1.5)$, $F = 1$.

recent LBT *ab initio* function produces A coefficients similar to those of LWR, but are in slightly poorer agreement with the present work. The Einstein coefficients of Turnbull and Lowe[10] and of Stevens *et al.*[12] are in considerable disagreement with those reported here. This is particularly evident in the $\Delta v = 2$ and $\Delta v = 3$ transitions (Figs. 5 and 6).

The dipole moment function reported in this work relies to a large extent on the measurement of the J dependent vibrational intensity variation induced by centrifugal distortion. It is therefore important that all other sources of J dependent intensity variation are accounted for in the interpretation of these results. There are two potentially important sources of additional J dependence due to electronic state interactions. These are the interaction between the two $^2\Pi$ states (spin uncoupling) and the interaction between the $X\,^2\Pi$ states and the excited $A\,^2\Sigma^+$ electronic state (L uncoupling). Spin uncoupling is a large effect in OH for $J \leqslant 10.5$ and is treated accurately in the analysis of our data.[17] The effects of L uncoupling on the OH rovibrational Einstein A coefficients are much smaller and are neglected in this analysis. Mies[13] has estimated the size of these effects which turn out to be significant only for J values much higher than observed in these studies and/or very weak transitions. Therefore, this problem is even only a potential concern for large $\Delta v = 1$ P/R intensity ratios where one transition is vanishingly weak. However, these ratios tend to be poorly determined due to sensitivity limitations and hence contribute proportionately less to the weighted least-squares fitting procedure. In all cases the random error uncertainties are much larger than the anticipated effects of interactions between the A and X electronic states.

TABLE XII. Previous experimental and theoretical predictions for OH($v = 0 \leftarrow 1$) radiative rates.

	Rotationless A(Hz) for $v = 0 \leftarrow 1$[a]
Experimental	
Benedict, Plyler[b] (1954)	33
D'Incan, Effantin, Roux[c] (1971)	8.5
Roux, D'Incan, Gerny[d] (1973)	42.5
Podolske, Johnston[e] (1983)	10.2
Turnbull, Lowe[f] (1988)	21.
Theoretical	
Meyer[g] (1974)	11.6
Stevens *et al.* (Mies)[h] (1974)	18.3
Werner, Rosmus, Reinsch[i] (1983)	12.2
Langhoff, Werner, Rosmus[j] (1986)	13.8
Present work	15.9(19)

[a] Corrected for rotational effects to facilitate comparison between different experimental and theoretical results.
[b] W. S. Benedict and E. K. Plyler, Natl. Bur. Stand. (U.S.), Circ. **523**, 57 (1954).
[c] J. D'Incan, C. Effantin, and F. Roux, J. Quant. Spectrosc. Radiat. Transfer **11**, 1215 (1971).
[d] F. Roux, J. D'Incan, and D. Gerny, Astrophys. J. **186**, 1141 (1973).
[e] J. R. Podolske and H. S. Johnston, J. Chem. Phys. **79**, 3633 (1983).
[f] D. N. Turnbull and R. P. Lowe, Planet. Space Sci. **37**, 723 (1989).
[g] Reference 11.
[h] Reference 13.
[i] H. Werner, P. Rosmus, and E. Reinsch, J. Chem. Phys. **79**, 905 (1983).
[j] Reference 14.

VI. INDEPENDENT EXPERIMENTAL TESTS OF $\mu(r)$

We offer two final and independent checks of the Einstein coefficients presented in this work. First, we can calculate the $\Delta v = 1/\Delta v = 2$ Einstein A ratios from an incomplete version of $\mu(r)$ based only upon a restricted data set *excluding* these $\Delta v = 1/\Delta v = 2$ ratios. In this way we allow the $\Delta v = 1$ P/R ratios to predict the $\Delta v = 1/\Delta v = 2$ ratios, thereby testing for an internal consistency in the determined $\mu(r)$. In Fig. 7 we compare the results of this prediction with the experimentally observed ratios. The agreement is excellent. Indeed, as is shown in Table VIII, the inclusion of the $\Delta v = 1/\Delta v = 2$ data in the fit changes $\mu(r)$ negligibly. This is an important observation since previous workers have relied on such $\Delta v = 1/\Delta v = 2$ relative intensity measurements in their investigations of the OH but with the analysis yielding a significantly different dipole moment function.[9,10] A key point of the above test is that the $\Delta v = 1/\Delta v = 2$ intensity ratios by themselves are not very sensitive to the slope of $\mu(r)$ near r_e. However, the combined set of $\Delta v = 1/\Delta v = 2$ and P/R branch J dependent intensity ratios, proves sufficient to determine $\mu(r)$ accurately. We also note that the consistency of the $\Delta v = 1$ P/R ratios with the $\Delta v = 1/\Delta v = 2$ ratios further implies that the effects of J dependent interactions with the A electronic state are unimportant. This follows because the $\Delta v = 1/\Delta v = 2$ measurements are made in the lowest two rotational states where J dependent interactions are completely negligible. Since these $\Delta v = 1/\Delta v = 2$ ratios are well predicted by the $\Delta v = 1$ P/R ratios, this suggests that the $\Delta v = 1$ P/R ratios are not significantly influenced by electronic state interactions either.

Our second check of internal consistency involves measuring the rotational/spin–orbit temperature of our emission source. The OH population in each rotational state is proportional to the amount of light emitted from that state, the proportionality constant being the Einstein A coefficient for the transition being monitored. Hence the population in

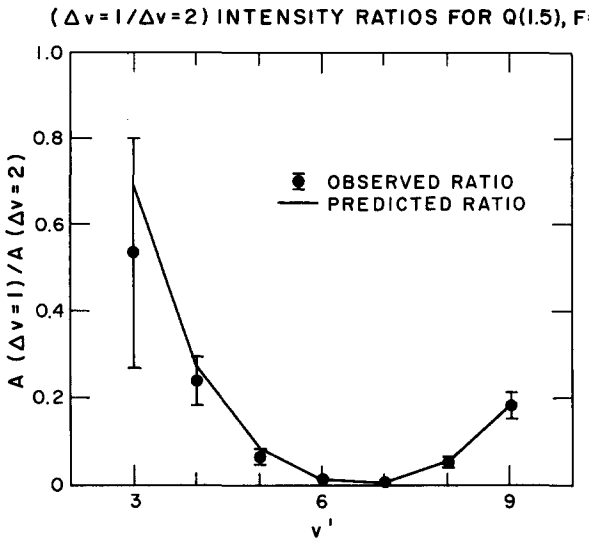

FIG. 7. Intensity ratios, $\Delta v = 1/\Delta v = 2$, for $Q(1.5)$, $F = 1$ as a function of v'. The solid line indicates the ratios predicted from a fit of $\mu(r)$ to just the $\Delta v = 1$ P/R ratios and permanent dipole moments. The solid circles show the experimental ratios which are in excellent agreement with the predictions.

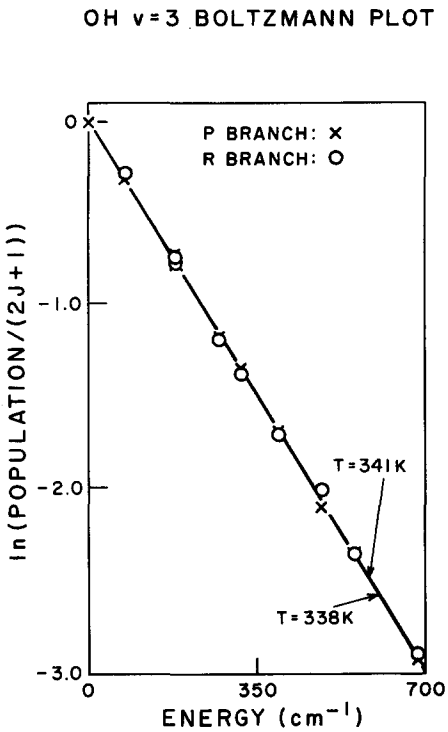

FIG. 8. Boltzmann plot of the rotational level population in OH($v = 3$) using the Einstein A coefficients reported in this work.

each J state, and thus an effective rotational temperature, can be measured independently using both P branch and R branch transitions as probes. We anticipate the establishment of rotational and spin–orbit equilibrium at a temperature only slightly higher than room temperature, since the OH radicals reside in the emission cell for ~ 10 ms in the presence of nearly 1 Torr of He and significant amounts of ozone. Since spin–rotation and uncoupling effects in OH lead to a large and different P and R branch dependence to the line strengths, errors in our dipole moment function may be evidenced in inconsistencies between effective P and R branch rotational temperatures.

Indeed, previous attempts to measure the rotational temperatures of OH emission sources which have not corrected for the strong J dependence of the A coefficients have resulted in an apparent temperature derived from P branch spectra with a significantly *different* apparent temperature being derived from R branch emission,[9] with discrepancies as large as 100 K. As appreciated at the time, the difficulties stem from an inability to correct the observed spectra for the marked J dependence of the Einstein A coefficients. In Fig. 8 we present Boltzmann plots of the populations of several rotational levels in $F = 1$ and $F = 2$ of $v = 3$ derived from our $v = 3 \rightarrow 2$ emission spectra. The populations are taken as the observed emission intensities corrected by the Einstein A coefficients reported in this work. The slopes of the P ($\times$ symbols) and R ($\bigcirc$ symbols) branch lines are identical within experimental uncertainty, indicating P and R branch temperatures in close agreement (338 ± 5 and 341 ± 5 K, respectively) and as anticipated, slightly higher than room temperature.

In contrast, if we correct the observed spectra with the Einstein coefficients derived from previous *ab initio* and empirical studies, the P and R branch results are dramatically less consistent. Table XIII shows the P and R branch temperatures obtained using several of the dipole moment functions discussed in this work, which yield P/R branch discrepancies on the order of 30–40 K. Figure 9 shows a Boltz-

TABLE XIII. Emission source rotational/spin orbit temperatures in $v' = 3$ obtained using several dipole moment functions.[a]

	P branch T_{rot} (K)	R branch T_{rot} (K)	$T^R_{rot} - T^P_{rot}$ (K)
Nelson *et al.* (this work)	338	341	3 ± 7
Mies[b]	337	370	33
Turnbull and Lowe[c]	346	306	−40
LWR[d]	331	374	43
LBT[e]	334	376	42

[a] Temperatures obtained from $v = 3 \rightarrow 2$ emission spectra corrected by Einstein coefficients of various workers.
[b] Based on Einstein A factors of Mies (Ref. 13) which he calculates from *ab initio* function of Stevens *et al.* (Ref. 12).
[c] Based on Einstein A factors which we calculate from empirical $\mu(r)$ of Turnbull and Lowe (Ref. 10).
[d] Based on Einstein A factors of Langhoff, Werner and Rosmus (Ref. 14).
[e] Based on Einstein A factors which we calculate from *ab initio* function of Langhoff, Bauschlicher, and Taylor (Ref. 15).

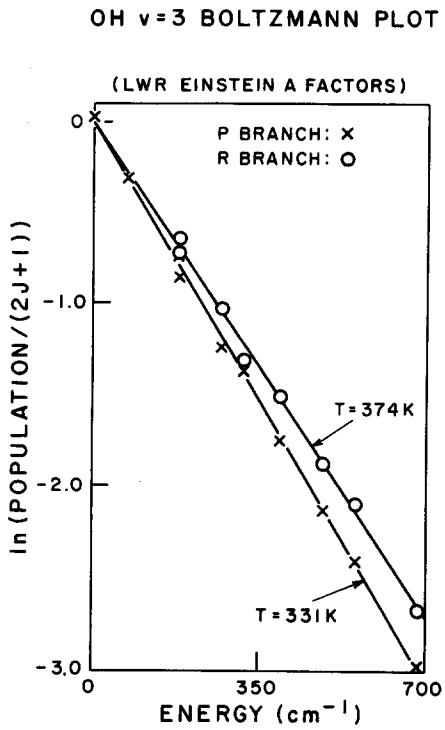

FIG. 9. Boltzmann plot of the rotational level population in OH($v = 3$) using the Einstein A coefficients reported by Langhoff *et al.* (Ref. 14).

mann plot of the P and R branch distributions obtained using the Einstein A coefficients of Langhoff *et al.*[14] Although these *ab initio* A coefficients of LWR are the closest to those which we report, these values still predict distinctly different P and R branch temperatures of 331 and 374 K. Besides P/R branch temperature discrepancies, the inferred populations also exhibit significant deviation from linearity in the Boltzmann plot that are absent in Fig. 8. We regard these additional tests of the rotational dependence of the Einstein A coefficients as strong independent support for the dipole moment function and Einstein A factors reported in this work.

Under these experimental conditions, rotational equilibration between the different vibrational manifolds is likely to be complete. As a further check, therefore, we use our Einstein A coefficients and observed emission signals in a standard Boltzmann analysis to determine the effective rotational temperature for *each* of the vibrationally excited states. The results obtained for P and R branches for $v' = 3$–7, $\Delta v = -1$ bands, are shown in Table XIV. The consistency of these rotational temperatures is excellent and well within the experimental uncertainty of each determination. This additional evidence strongly supports these A coefficients as the most reliable for precise characterization of OH population distributions.

As a final note of interest, we have also briefly analyzed the *integrated* band intensities for each vibrational level, summed over all rotational levels. These populations vary by a factor of 15 from $v = 1$ to $v = 9$, and yield a surprisingly

TABLE XIV. Consistency of emission source rotational/spin–orbit temperatures for $v' = 3$–7 obtained from the Nelson *et al.* OH dipole moment function.

v'	v''	P branch T_{rot} (K)	R branch T_{rot} (K)
3	2	338(5)	341(5)
4	3	342(5)	361(40)[a]
5	4	336(5)	[b]
6	5	349(7)	[b]
7	6	[b]	336(7)
		$\langle T_{rot}\,(K)\rangle = 340(5)$	

[a] Larger uncertainty in temperature due to small Einstein A coefficients for this branch.

[b] Insufficient S/N ratio due to vanishingly small Einstein A coefficients in these branches for the most thermally populated J states.

linear Boltzmann plot well characterized by a vibrational temperature of 12 500 K. There is no *a priori* reason to expect such a simple distribution of vibrational levels in the spectrometer. Of course, this distribution is far from nascent due to collisional and reactive relaxation processes, but is evidently much hotter than T_{rot} due to less efficient vibrational vs rotational energy transfer processes.

VII. SUMMARY AND CONCLUSION

The Einstein A coefficients presented in this work permit the measurement of OH quantum state populations directly from emission observations. This statement is convincingly illustrated in the rotational/spin–orbit Boltzmann plot of Fig. 8 discussed above. Further efforts to confirm the OH dipole moment function include measurement of the OD emission spectra by FTIR techniques and the measurement of the absolute intensities of OH $v = 2 \leftarrow 0$ transitions in absorption using a color center laser. These results represent an important step in the attempt to unravel the complex kinetics of vibrationally excited OH radicals in the mesosphere from ground based emission measurements. Ongoing research efforts in our laboratories are exploiting these absolute Einstein A coefficients to measure energy transfer rates of highly rotationally and vibrationally excited OH, as well as to investigate the effects of vibrational excitation on the reactivity of this chemically important species. The present measurement of precise OH Einstein A coefficients should greatly accelerate our quantitative understanding in both laboratory and field based studies of the intriguing atmospheric phenomena involved in the OH night glow.

ACKNOWLEDGMENTS

The work at JILA has been supported by grants from the Air Force Office of Scientific Research. D.D.N. gratefully acknowledges the National Research Council for a Resident Research Associateship. D.J.N. thanks the Sloan Foundation for his Sloan Fellowship. The work at NOAA was supported in part by the National Aeronautics and Space Administration Upper Atmosphere Program.

[1] A. B. Meinel, Astrophys. J. **111**, 555 (1950); **112**, 120 (1950).
[2] E. J. Llewellyn, B. H. Long, and B. H. Solheim, Planet. Space Sci. **26**, 525 (1978).
[3] E. A. Lyttle and J. Hampson, Nature **202**, 76 (1964).
[4] J. L. Hall, D. Zeitz, J. W. Stephens, J. V. V. Kasper, G. P. Glass, R. F. Curl, and F. K. Tittel, J. Phys. Chem. **90**, 2501 (1986).
[5] D. D. Nelson, Jr., A. Schiffman, and D. J. Nesbitt, J. Chem. Phys. **90**, 5455 (1989); A. Schiffman, D. D. Nelson, Jr., M. Pirkey, and D. J. Nesbitt (in preparation).
[6] N. Grevesse, A. J. Sauval, and E. F. van Dishoeck, Astron. Astrophys. **141**, 10 (1984).
[7] V. V. Smith and D. L. Lambert, Astrophys. J. **311**, 843 (1986).
[8] D. Garvin, H. P. Broida, and H. J. Kostkowski, J. Chem. Phys. **32**, 880 (1960).
[9] R. E. Murphy, J. Chem. Phys. **54**, 4852 (1971), and references therein.
[10] D. N. Turnbull and R. P. Lowe, J. Chem. Phys. **89**, 2763 (1988).
[11] W. Meyer, Theoret. Chim. Acta **35**, 277 (1974).
[12] W. J. Stevens, G. Das, A. C. Wahl, D. Neumann, and M. Krauss, J. Chem. Phys. **61**, 3686 (1974).
[13] F. H. Mies, J. Mol. Spectrosc. **53**, 150 (1974).
[14] S. R. Langhoff, H. Werner, and P. Rosmus, J. Mol. Spectrosc. **118**, 507 (1986); IR chemiluminescence studies by B. S. Agrawalla, A. S. Manocha, and D. W. Setser [J. Phys. Chem. **85**, 2873 (1981)] tend to support the Langhoff predictions of Einstein A coefficients versus the earlier calculations by Mies.
[15] S. R. Langhoff, C. W. Bauschlicher Jr., and P. R. Taylor, J. Chem. Phys. **91**, 5953 (1989).
[16] K. I. Peterson, G. T. Fraser, and W. Klemperer, Can. J. Phys. **62**, 1502 (1984).
[17] D. D. Nelson Jr., A. Schiffman, D. J. Nesbitt, and D. J. Yaron, J. Chem. Phys. **90**, 5443 (1989).
[18] J. B. Burkholder, P. D. Hammer, and C. J. Howard, J. Phys. Chem. **91**, 2136 (1987).
[19] D. L. Baulch, R. A. Cox, P. J. Crutzen, R. F. Hampson Jr., J. A. Kerr, J. Troe, and R. T. Watson, J. Phys. Chem. Ref. Data **11**, 362 (1982).
[20] J. C. Polanyi and J. J. Sloan, Int. J. Chem. Kin. Sym. **1**, 51 (1975).
[21] H. Ohoyama, T. Kasai, Y. Yoshimura, H. Kimura, and K. Kuwata, Chem. Phys. Lett. **118**, 263 (1985).
[22] J. E. Spencer and G. P. Glass, Chem. Phys. **35**, 15 (1976).
[23] D. L. Baulch, R. A. Cox, R. F. Hampson Jr., J. A. Kerr, J. Troe, and R. T. Watson, J. Phys. Chem. Ref. Data **13**, 1352 (1984).
[24] I. W. M. Smith and M. D. Williams, J. Chem. Soc., Faraday Trans. 2 **81**, 1849 (1985).
[25] J. A. Coxon and S. C. Foster, Can. J. Phys. **60**, 41 (1982); J. A. Coxon, *ibid.* **58**, 933 (1980).
[26] G. Guelachvili and K. N. Rao, *Handbook of Infrared Standards* (Academic, New York, 1986).
[27] T. Amano, J. Mol. Spectrosc. **103**, 436 (1984).
[28] See AIP document no. PAPS JCPSA-94-7003-9 for 9 pages of the complete versions of Tables IX, X, and XI. Order by PAPS number and journal reference from American Institute of Physics, Physics Auxiliary Publication Service, 335 East 45th Street, New York, NY 10017. The price is $1.50 for each microfiche (98 pages) or $5.00 for photocopies of up to 30 pages, and $0.15 for each additional page over 30 pages. Airmail additional. Make checks payable to the American Institute of Physics.